ONLINE FIRST

Folia Histochemica et Cytobiologica

ISSN: 0239-8508

e-ISSN: 1897-5631

Periplaneta americana extract attenuates hepatic fibrosis progression by inhibiting collagen synthesis and regulating the TGF-β1/Smad signaling pathway

Authors: Yi Chen, Yanwen Zhao, Liping Yuan, Ying He, Yongshou Yang, Peiyun Xiao

DOI: 10.5603/fhc.94457

Article type: Original paper

Submitted: 2023-03-01

Accepted: 2023-11-13

Published online: 2023-12-01

ORIGINAL PAPER

Periplaneta americana extract attenuates hepatic fibrosis progression by inhibiting collagen synthesis and regulating the TGF-β1/Smad signaling pathway

Short running title: *Periplaneta americana* extract attenuates liver fibrosis

Yi Chen[1, 2], Yanwen Zhao[1, 3], Liping Yuan[1], Ying He[1], Yongshou Yang[1*], Peiyun Xiao[1*]

[1]Yunnan Provincial Key Laboratory of Entomological Biopharmaceutical R&D, College of Pharmacy, Dali University, Dali, Yunnan, China

[2]Affiliated Hospital of Panzhihua University, Panzhihua, Sichuan, China

[3]Mangshi Maternal and Child Health Care Hospital, Dehong, Yunnan, China

Address for correspondence:

Yongshou Yang and Peiyun Xiao

College of Pharmacy, Dali University, Dali City, Dali, Yunnan, 671000, China

e-mails: yangyongshou@dali.edu.cn (Y.Yang); xiaopeiyun@dali.edu.cn (P.Xiao)

Submitted: 1 March, 2023

Accepted after reviews: 13 November, 2023

Available as AoP: 1 December, 2023

Abstract

Introduction. Liver fibrosis is the damage repair response following chronic liver diseases. Activated hepatic stellate cells (HSCs) are the main extracellular matrix (ECM)-producing cells and key regulators in liver fibrosis. *Periplaneta americana* shows prominent antifibrotic effects in liver fibrosis; however, the underlying mechanisms remain undetermined. This study aimed to elucidate the therapeutic effects of *P. americana* extract (PA-B) on liver fibrosis based on the regulation of the TGF-β1/Smad signal pathway.

Material and methods. HSCs and Sprague Dawley rats were treated with TGF-β1 and CCl_4, respectively, to establish the hepatic fibrosis model *in vitro* and *in vivo*. The effect of PA-B on

liver rat fibrosis was evaluated by biochemical (serum aspartate aminotransferase (AST), alanine aminotransferase (ALT), hyaluronic acid (HA), laminin (LN), collagen type Ⅳ (Col-Ⅳ), pro-collagen type Ⅲ (PC-Ⅲ)) and histological examinations. Further, fibrogenic markers expression of alpha smooth muscle actin (α-SMA), collagen type I (Col-I), and collagen type III (Col-III), and the TGF-β1/Smad pathway-related factors were assessed by immunofluorescence (IF), real time quantitative polymerase chain reaction (RT-qPCR), and western blotting (WB).

Results. Treatment of HSC-T6 cells with PA-B suppressed the expression of α-SMA, Col-I, and Col-III, downregulated the expression of TGF-β1 receptors I and II (TβR I and TβR II, respectively), Smad2, and Smad3, and upregulated Smad7 expression. PA-B mitigates pathologic changes in the rat model of liver fibrosis, thus alleviating liver index, and improving liver function and fibrosis indices. The effects of PA-B on the expression of α-SMA, Col-I, Col-III, TβR I, TβR II, Smad2, Smad3, and Smad7 were consistent with the *in vitro* results, including reduced TGF-β1 expression.

Conclusions. The therapeutic effect of PA-B on liver fibrosis might involve suppression of the secretion and expression of TGF-β1, regulation of the TGF-β1/Smad signaling pathway, and inhibition of collagen production and secretion.

Keywords: liver fibrosis; *Periplaneta americana* extract; HSC-T6 cells; collagen type I; collagen type III; TGF-β1/Smad pathway

Introduction

Liver fibrosis is a tissue repair process of numerous chronic liver diseases, including non-alcoholic steatohepatitis, cholestasis, viral hepatitis, autoimmune hepatitis, and so on [1]. Liver fibrosis is a necessary pathological process of cirrhosis and liver failure. About 2 million patients die of liver fibrosis or cirrhosis in the world every year, and the case-fatality rate caused by complications has been high in recent years, increasing the economic burden on families and society [2]. However, there is no specific drug to cure liver fibrosis at present [1]. Therefore, research and development of safe and effective therapeutic drugs with less adverse reactions is still a clinical problem for the treatment of liver fibrosis.

Liver fibrosis is caused by the imbalance of extracellular matrix (ECM) synthesis and degradation. Hepatic stellate cells (HSCs) activation is the key link within the advancement of liver fibrosis. HSCs are specialized perihepatic cells located in the Disse space within the liver sinusoid [3]. HSCs are responsible for maintaining ECM homeostasis and storing vitamin A in the form of retinyl esters within cytoplasmic lipid droplets, under normal physiological conditions [4]. However, following liver injury, they are activated and phenotypically transformed into myofibroblasts, leading to excessive accumulation of the ECM [5–8]. Platelets discharge excess

transforming growth factor-β1 (TGF-β1) post injury in the liver cell, which enhances activation of HSCs. Activated HSCs promote ECM synthesis and accumulation [9, 10]. Notably, activated HSCs also enhance the synthesis and secretion of TGF-β1, and further promote liver fibrosis [11, 12]. TGF-β1 is a crucial promoter of the TGF-β/Smad signaling pathway [13]. The TGF-β family exercises its biological effects via this pathway, which is implicated in the regulation of various cellular activities including activation of transmembrane receptors, collagen transcription, regulation of cell separation, apoptosis, and migration [14, 15]. Recently, the TGF-β/Smad signaling pathway was utilized as an effective target for fibrosis treatment [16–18].

Traditional Chinese medicine is utilized to handle a wide range of maladies, as evidenced by its great effectiveness and safety over a long periods of clinical use. *Periplaneta americana* L. is a precious traditional Chinese medicine, which was initially recorded in *Shen Nong's Herbal Classic* nearly 2000 years ago. Modern research has indicated that *Periplaneta americana* mainly contains proteins, peptides, polyols, and aliphatic acids, and has various biological and pharmacological properties including tissue repair, anti-inflammatory, antioxidant, anti-fibrosis, and hepatoprotective effects [19–23]. A previous study of our research team found that *Periplaneta americana* extract (PA-B) reduced the expression of four indices of liver fibrosis in CCl_4 model rats, indicating that it can be used as a therapy for liver fibrosis [24, 25]. However, the anti-fibrosis effect and underlying mechanisms of PA-B remain poorly understood. This study aimed to determine the degree of collagen and correlation factor expression in the TGF-β1/Smad signaling pathway in HSC-T6 cells and hepatic fibrosis rat liver. The molecular mechanism of anti-liver fibrosis effects by PA-B were determined to enable a better understanding of treating liver fibrosis.

Material and methods

Reagents and antibodies. Colchicine was acquired from Yunnan Plant Pharmaceutical Co., Ltd. (Nanjing, China). Carbon tetrachloride was purchased from Tianjin Fuchen Chemical Reagent Factory (Tianjin, China). PeproTech provided recombinant human TGF-β1 (Westlake Village, CA, USA). Aminotransferase (AST), alanine aminotransferase (ALT), hyaluronic acid (HA), laminin (LN), procollagen-III (PC-III), and type IV collagen (Col-IV) assay kits were acquired from Nanjing Jiancheng Bioengineering Institute (Nanjing, China). Diaminobenzidine (DAB) chromogen kit, 4′,6-diamidino-2-phenylindole (DAPI), Radio-Immunoprecipitation Assay (RIPA) lysis buffer, and bicinchoninic acid assay (BCA) kit were purchased from Solarbio (Beijing, China). LY364947 was acquired from Sigma (MO, USA). TRIzol™ reagent was obtained from Invitrogen (Carlsbad, CA, USA). RevertAid™ first strand cDNA synthesis kit was obtained from Thermo Fisher Scientific (Waltham, MA, USA). SYBR Green master mix was obtained from

Takara (Tokyo, Japan). Primers were purchased from Shanghai Sangon Biological Engineering Co., Ltd. (Shanghai, China). Anti-α-SMA (ab124964), anti-collagen I (ab34710), anti-collagen III (ab7778), Cy5-labeled goat anti-rabbit IgG H&L Cy5 (ab6564), anti-TβR I (ab235578) and anti-Smad7 (ab216428) were obtained from Abcam (Cambridge, UK). GAPDH (5174S), Anti-TβR II (79424S), anti-Smad2 (5339S), and anti-Smad3 (9523S) were obtained from Cell Signaling Technology (Danvers, MA, USA). Goat anti-rabbit IgG-horseradish peroxidase (SA00001-2) was obtained from Proteintech (Wuhan, China). Enhanced chemiluminescence kit (ECL) was obtained from Beyotime Biotechnology (Nanjing, China).

Preparation of PA-B. *Periplaneta americana* was collected from Yunnan Jingxin Biological Technology Co. Ltd. and authenticated by Dr. Z Yang of Key Laboratory of Insect Biomedical Research and Development, Dali University, Yunnan Province, China. Voucher specimens of the insect visitors are deposited in the Herbarium of Dali University (No. 2018.06.24).

The following procedure was used to extract PA-B (freeze-dried powder). The extraction was carried out three times with 70% aqueous ethanol at 80℃ (2.5 h per time). The extract was then loaded onto a polyamide column and eluted with water and various quantities of aqueous ethyl alcohol before being quantitatively collected and concentrated separately. This extract was freeze-dried and used in further experiments. At the same time, the quality control methods were used for testing, as previously described by Fu *et al*. [26].

Separation and identification. PA-B extract was adjusted to 20 mg/mL with methanol and separated by semi-preparative high performance liquid chromatography (HPLC) according to previously described chromatographic conditions [26]. Hydrogen and carbon spectra of the compounds were determined using a Bruker Avance III HD 400 nuclear magnetic resonance (NMR) spectrometer (Bruker Corporation, Billerica, USA, QNP $^{1}H/^{13}C/^{19}F/^{31}P$ probe, 400.13 MHz).

Cell culture. The Cell Bank of Chinese Academy of Sciences provided HSC-T6 cells (an immortalized strain of rat HSCs) (Shanghai, China). HSC-T6 cells were maintained at 37°C and 5% CO_2 in Dulbecco's modified Eagle's medium (DMEM, Gibco, Thermo Fisher Scientific, Inc.) with 10% fetal calf serum (FBS, Gibco, Thermo Fisher Scientific, Inc.) and 100 U/mL penicillin-streptomycin (Beijing Solarbio Science and Technology Co., Ltd.). Cells were passaged at a density of 70–80%. The medium was replaced every other day.

Establishment of the TGF-β1 activated HSC-T6 cells model and drug treatments. Cells were seeded at 6×10^4 cells/mL on culture plates before treatment. HSC-T6 cells were cultured for 24 h, then treated with multiple concentrations of PA-B, TGF-β1 and LY-364947 (a diheteroaryl-substituted pyrazole compound used as a selective, ATP-competitive inhibitor of TGF-β Receptor I kinase) for a further 24 h. The following groups of HSC-T6 cells were established: 1) control; 2)

TGF-β1 (10 ng/mL); 3) TGF-β1 (10 ng/mL) + LY-364947 (50 μmol/L); 4) TGF-β1 (10 ng/mL) + PA-B (50 μg/mL); 5) TGF-β1 (10 ng/mL) + PA-B (60 μg/mL); 6) TGF-β1 (10 ng/mL) + PA-B (70 μg/mL). The concentration of the PA-B storage solution was 30 mg/mL. The PA-B stock was diluted 10 times using DMEM with 1% FBS and further diluted to the desired concentration for use.

Experimental animals. Forty-eight six-week-old male Sprague Dawley rats weighing 180–200 g were purchased from Hunan SJA Laboratory Animal Technology, Co., Ltd. (Hunan, China) [Animal License No. SCXK (Xiang) 2019-0004]. The rats were kept in a typical 12 h light/dark cycle at 21 ± 2℃ and 60 ± 5% humidity with unrestricted access to food and water. The animal experiments adhered to the guidelines set out by the school's animal ethics committee.

Establishment of the CCl_4-induced liver fibrosis model and drug treatment. Rats were acclimatized for 1 week before being randomly assigned into 6 groups (8 rats per group): (1) control; (2) CCl_4 (1 mL/kg); (3) CCl_4 (1 mL/kg) + colchicine (0.2 mg/kg); (4) CCl_4 (1 mL/kg) + PA-B (30 mg/kg); (5) CCl_4 (1 mL/kg) + PA-B (60 mg/kg); (6) CCl_4 (1 mL/kg) + PA-B (120 mg/kg). The control rats were intraperitoneally injected with corresponding dose of olive oil (2 mL/kg or 1 mL/kg), whereas the CCl_4, colchicine, and PA-B groups were administered in 40% CCl_4 oil solution (diluted with olive oil, first injection at a dose of 2 mL/kg and maintained at a dose of 1 mL/kg) twice a week for a duration of six weeks. After HE staining revealed that the liver fibrosis model was successfully established, the following protocol was performed by gavage administration once a day for 4 weeks: the control and CCl_4 groups were administered an equal volume of 0.5% sodium carboxymethyl cellulose (CMC-Na) solution, while the colchicine group was given colchicine (0.2 mg/kg, suspended in 0.5% CMC-Na), and the PA-B treatment groups were administered different concentrations of PA-B (30, 60, and 120 mg/kg, suspended in 0.5% CMC-Na), respectively.

The animals were anesthetized with 1% sodium pentobarbital (5.5 mL/kg) after 24 h fasting following the conclusion of the treatment. Serum samples were collected and stored at –80°C for subsequent experiments. The liver was promptly separated before removing surrounding fat and connective tissue, then accurately weighed. The changes of liver mass in proportion to body's mass was evaluated by the liver index formula: liver weight (g)/body weight (g). Part of the liver was fixed in 4% paraformaldehyde for 24 h to prepare histological sections. The remaining parts and tissues were preserved at –80°C.

Serum liver function index and parameters of liver fibrosis. Commercial kits were used to test serum AST and ALT activities according to the manufacturer's instructions. The levels of HA, LN, PC-III, and Col-IV in rat serum were measured using enzyme linked immunosorbent assay (ELISA) kits according to the procedures (Nanjing Jiancheng Bioengineering Institute).

Histopathological analysis. Liver samples were fixed in 4% paraformaldehyde, embedded in paraffin, and cut into 5 μm-thick slices. Samples were stained with hematoxylin and eosin (H&E) and Masson's trichrome stain [27, 28]. Subsequently, the morphological alterations of liver tissues of rats were evaluated by an optical microscope (CX31, Olympus, Tokyo, Japan).

Immunofluorescence staining analysis. HSC-T6 cells were seeded in 24-well plates and treated with TGF-β1. Cells were collected after 24 h, 48 h, and 72 h of culturing with LY364947 and PA-B of designed concentrations. Cells were fixed with 4% paraformaldehyde, then permeabilized with 0.1% Triton X-100. Permeabilized cells were blocked with 3% albumin, then incubated overnight at 4℃ with primary antibodies diluted to 1:200 using phosphate buffered saline (PBS). HSC-T6 cells were rinsed with PBS, incubated with anti-rabbit IgG (Cy5-labeled, diluted in PBS, 1:1000) at 25 ± 5℃, then counterstained with DAPI (diluted in PBS, 1:100). Images were captured using a Leica TCS SP8 STED confocal microscope (Weztlar, Germany).

Immunohistochemistry and quantitative analysis. Liver tissue sections were de-waxed and rehydrated. HSC-T6 cells were grown on coverslips as for horizontal climbing slices, then cultured with various concentrations of TGF-β1, LY-364947, and PA-B for 24 h. The sections and slices were blocked with 0.3% H_2O_2 solution and treated with 5% (w/v) bovine serum albumin (BSA) to prevent nonspecific protein binding, then incubated with primary antibodies (TβRI = 1:500, TβRII = 1:200, Smad2 = 1:100, Smad3 = 1:100, Smad7 = 1:500), diluted in 1% (w/v) BSA overnight at 4℃, followed by incubation with secondary antibody (1:1000, diluted in 1% (w/v) BSA for 30 min at 37℃ in an incubator. Finally, DAB was used to visualize proteins and nuclei were re-stained with hematoxylin. Image-Pro Plus 6.0 (Media Cybernetics Inc, Rockville, MD, USA) was used to perform immunohistochemical quantification of positive regions, and the quantitative results were expressed by integrated optical density (IOD) values.

RNA isolation and real time quantitative polymerase chain reaction (RT-qPCR) analysis. TRIzol™ reagent was used to isolate total RNA from HSC-T6 cells and liver samples. Chloroform, isopropanol, ethanol, and other reagents were used for purification and further separation of RNA. A certain amount of RNA was reverse transcribed into cDNA for 5 min at 25°C, 60 min at 42°C, and 5 min at 70°C [29]. cDNA was amplified using SYBR Green master mix. The primer sequences are listed in Table 1. The cycling conditions were as follows: initial denaturation at 95℃ for 30 s, followed by 48 cycles of denaturation at 95℃ for 5 s, annealing for 5 s, and extension at 60℃ for 30 s. RT-qPCR analysis was performed with the Bio-Rad CFX96™ real-time system. The $2^{-\Delta\Delta Ct}$ method was used to analyze the data and normalized to GAPDH as a control.

Protein isolation and western blot analysis. RIPA lysis buffer was added to HSC-T6 cells and liver samples to isolate total proteins. The supernatant protein concentration was determined using

a bicinchoninic acid assay (BCA) kit. Each sample was adjusted to the same protein concentration. The proteins were separated by 10% sodium dodecyl sulfate polyacrylamide gel electrophoresis (SDS-PAGE), and immediately transferred to a polyvinylidene difluoride (PVDF) membrane. The membrane was blocked with 5% (w/v) skim milk at 25 ± 5℃ for 2 h, then incubated with primary antibodies (GAPDH = 1:1000, TβRI = 1:1000, TβRⅡ = 1:500, Smad2 = 1:1000, Smad3 = 1:1000, Smad7 = 1:1000), diluted in 1% (w/v) BSA at 4℃ overnight. The membranes were washed with Tris buffered saline Tween 20 (TBST), then incubated with the appropriate secondary antibody. The membranes were then scanned with an enhanced chemiluminescence kit (ECL). The band intensity was performed using Image J (National Institutes of Health, Bethesda, MD, USA), with the results compared to the intensity of GAPDH.

Statistical analysis. The data was processed by SPSS26.0 (SPSS Inc., Chicago, IL, USA). Data that conformed to the normal distribution were depicted as the mean ± standard deviation (SD), and the analysis of variance (ANOVA) was adopted for comparisons in three or more groups. Graph Pad Prism 6 (Graph Pad Software, San Diego, CA) was performed for all analyses. A P value of < 0.05 was treated as statistically significant.

Results

Semi-preparative HPLC identified compound structures in PA-B 9

The 9 purified compounds from PA-B were isolated by semi-preparative HPLC (Fig. 1). They were identified according to the results of ^{1}H- and ^{13}C-NMR (Table 2).

PA-B attenuates the liver index and biochemical indices of liver fibrosis induced by CCl_4 in rats

The liver index and biochemical indices were evaluated in the serum of rats with liver fibrosis to evaluate the effect of PA-B. Compared with the control group, the liver index of the CCl_4-treated rats increased significantly (Fig. 2A). Compared with the CCl_4 group, the liver index decreased after treatment with colchicine and PA-B. It is worth noting that the colchicine and PA-B intervention reduced the liver index, but it was still higher than in the control group. However, it decreased as compared with the model group after middle and high dose of PA-B (60 mg/kg and 120 mg/kg). There was no difference in liver index between the PA-B (60 mg/kg and 120 mg/kg) intervention group and the control group.

As shown in Fig. 2B, the serum activity of AST was considerably greater in the CCl_4-induced animals than those in the control group. Following PA-B treatment with the middle and high PA-B doses (60 mg/kg and 120 mg/kg), the CCl_4-induced animals showed decreased AST serum activity, in contrast to rats that received colchicine and the lowest PA-B dose. Similarly to changes of the serum AST activities, the serum activities of ALT were significantly higher in CCl_4-induced

animals than that of the control group (Fig. 2C). After the treatment with colchicine and all doses of PA-B, levels of ALT activity became markedly reduced .

Serum levels of four liver fibrosis markers (HA, LN, PC-III, and Col-IV) (Fig. 2D–G) were higher in CCl_4-induced rats compared with the control group; however, their concentrations decreased after colchicine and PA-B treatment at each PA-B dosage as compared with the CCl_4-treated rats. This indicated that PA-B alleviates suppression of liver function and decreases the indices of liver fibrosis in CCl_4-induced rats.

PA-B attenuates the pathological changes in the fibrotic liver of CCl_4-treated rats

The sections of the rat liver were evaluated to assess the effects of PA-B on experimental hepatic fibrosis (Fig. 3). The control group exhibited normal hepatocyte structure, and the central vein was clearly delineated with radiating hepatic cords of cells. In contrast, in the CCl_4 group inflammatory cell infiltration and pseudo-lobule formation were clearly visible, accompanied by hepatic cords disappearance and karyolysis (Fig. 3). In the colchicine group, hepatocyte disarray, inflammatory cell infiltration and disordered hepatocyte cords arrangement were observed. Treatment with the middle and high doses of PA-B caused a dose-dependent partial attenuation of the liver structure alterations compared with the CCl_4 group.

The shape and distribution of collagen fibrosis was observed by Masson's staining to further examine the effect of PA-B on CCl_4-induced liver fibrosis (Fig. 3). In the control group there was only minimal staining of collagen fibers in portal areas and around central veins, and the hepatic lobule structure was normal. In the CCl_4 group collagen fibers proliferated around the portal spaces, and the collagen fibers in different portal areas were connected to each other to form pseudo-lobular formations (Fig. 3). Compared with the CCl_4 group, the arrangement of collagen fiber bundles did not decrease in the colchicine group. However, the collagen fibers staining was reduced to different degree amongst the PA-B groups and the effect of the PA-B at 120 mg/kg was the most significant.

PA-B attenuates the expression of fibrogenic markers in HSC-T6 cells

In the TGF-β1-exposed HSC-T6 cells, immunofluorescence staining clearly showed α-SMA red fluorescence which was randomly distributed throughout the cytoplasm, and most intensely expressed after 24 h (Fig. 4A, B). Similarly, Col-I (Fig. 4C) and Col-III (Fig. 4E) were mainly distributed in the cytoplasm, however, the intensity of Col-I immunostaining was much higher than that of Col-III (Fig. 4D *vs.* 4F). Thus, α-SMA, Col I and Col III stainings indicated that TGF-β1 activated cultured HSC-T6 cells. The immunofluorescence intensity of α-SMA, Col-I, and Col-III in TGF-β1-exposed HSC-T6 cells significantly decreased with increasing PA-B

concentrations. In addition, the LY-364947 group showed the same trend as did the PA-B treatment groups (Fig. 4A–F).

PA-B attenuates expression of fibrogenic markers in the liver of rats with experimental fibrosis

Immunohistochemistry was used to localize the expression of fibrogenic markers in the liver to evaluate the effect of PA-B on experimental hepatic fibrosis. Almost no expression of α-SMA and COL-I was found in the liver of control rats (Fig. 5A, B). In the liver of the CCl_4 group α-SMA was highly expressed in portal tracts between pseudo-lobuli (Fig. 5A), whereas Col-I was expressed mainly in the portal tract areas (Fig. 5B). The expression of α-SMA and Col-I in the colchicine group and PA-B (30 mg/kg) groups appeared to be lower than that in the CCl_4 group even if not confirmed by integrated optical density measurements. Apparently, the hepatic immunoreactivity of α-SMA and Col-I was drastically reduced in the middle and high PA-B groups (60 mg/kg and 120 mg/kg) (Fig. 5A–C).

The mRNA levels of α-SMA and Col-I increased to varying degrees in rat liver after CCl_4 treatment compared with the control group (Fig. 5D, E). Treatment of rats with induced fibrosis with PA-B and colchicine led to decreased hepatic α-SMA and Col-I mRNA levels, and these changes were especially conspicuous in rats treated with the highest dose of PA-B (120 mg/kg). Thus, PA-B considerably decreased the mRNA expression level of collagen in hepatic fibrosis rats.

Administration of PA-B inhibits the TGF-β/Smad pathway in HSC-T6 cells

The expression of TGF-β receptors type I and II (TβR I, TβR II), and their key signaling factors (Smad2, Smad3, and Smad7) were examined by immunohistochemistry to investigate the effects of PA-B in HSC-T6 cells through the TGF-β/Smad pathway (Fig. 6A, B). The immunoreactivity (Ir) of TβR I and TβR II increased in TGF-β1-induced HSC-T6 cells, as did the downstream Smad2 and Smad3 expression. Besides, the Smad7-Ir in TGF-β-exposed HSC-T6 cells was considerably decreased. The LY-364947- and PA-B-treated cells exhibited reduced expression levels of TβR I, TβR II, Smad2, and Smad3 proteins, and increased expression level of Smad7, compared with the TGF-β1 group. Western blot results corresponded with those of immunohistochemistry (Fig. 6C, E).

In addition, mRNA expression of TβR I, TβR II, Smad2, and Smad3 drastically increased in TGF-β1-induced HSC-T6 cells, while the Smad7 mRNA expression was decreased (Fig. 6D). After treatment of TGF-β1-induced HSC-T6 cells with LY-364947 and PA-B, the mRNA levels of TβR I, TβR II, Smad2 and Smad3 were considerably decreased whereas that of Smad7 was increased.

Administration of PA-B inhibits the TGF-β/Smad pathway in liver fibrosis rats

The expression levels of key signaling factors (TβR I, TβR II, Smad2, Smad3, TGF-β1, and Smad7) were examined by RTqPCR and western blotting to investigate the effects of PA-B on liver fibrosis by analyzing the TGF-β/Smad pathway. The mRNA expression of TβR I, TβR II, Smad2, Smad3, and TGF-β1 was significantly higher in the CCl_4 group compared with the control group, and Smad7 mRNA expression was evidently lower (Fig. 7A). After PA-B and colchicine treatment the mRNA expression of TβR I, TβR II, Smad2, Smad3, and TGF-β1 was significantly decreased in liver tissues, and that of Smad7 was significantly increased.

Western blotting (Fig. 7B, C) showed that the protein expression of TβR I, TβR II, Smad2, and Smad3 were much higher in the liver of CCl_4-induced rats than in the control group, and Smad7 protein expression was significantly decreased. The expression of TβR I, TβR II, Smad2, and Smad3 decreased in the liver after PA-B and colchicine treatment. The greatest changes were observed in the PA-B group at 120 mg/kg, while Smad7 protein increased compared with the CCl_4 group. These results matched those of the RT-qPCR assays (Fig. 7B, C).

Discussion

The occurrence and development of liver fibrosis is closely linked to the imbalance of ECM synthesis and degradation in liver tissue [30]. Liver damage causes hepatocytes and Kupffer cells to produce pro-fibrotic and pro-inflammatory factors to activate resting HSCs [31]. Activated HSCs increase ECM secretion, which results in excessive ECM deposition [32].

Periplaneta americana L has been found to be effective in preventing fibrogenesis and chronic liver injury [33, 34]. PA-B is an anti-fibrosis active component extracted from *Periplaneta americana* L. Our group has been trying to unravel the main components in PA-B, and isolated 9 compounds [26]. At the experimental dose of 40–120 μg/mL, the inhibitory effect of compound 1 (IC_{50} = 67.03 μg/mL) and compound 3 (IC_{50} = 70.46 μg/mL) on HSC-T6 was slightly better than that of PA-B (IC_{50} = 75.29 μg/mL), but there was no significant difference, and their proportion was very low (1.63%, 0.30%). While compounds 4 and 5 had poor inhibitory effect on HSC-T6 cells, and other compounds had no effect on the proliferation. Therefore, we speculated that the inhibitory effect of PA-B on HSC-T6 cell proliferation was the result of multi-component synergic action. Based on the above factors, PA-B was selected to study the mechanism of anti-liver fibrosis in subsequent experiment.

Colchicine is an alkaloid extracted from *Colchicum autumnale* L. that has anti-gout and anti-inflammatory effects. Many studies demonstrated that colchicine can counteract hepatocytes' damage by inhibiting the activation and proliferation of HSCs, promoting collagen degradation,

inhibiting excessive ECM deposition, and reducing hepatic peroxidation damage. Therefore, colchicine was selected as an established anti-fibrotic drug in this study [35, 36].

TGF-β1 is a major cytokine that induces liver fibrosis by initiation and activation of HSCs [37, 38]. CCl_4 directly destroys the liver cell membrane resulting in necrosis of hepatocytes and liver fibrosis [39, 40]. The liver damage caused by CCl_4 is very similar to human liver disease in morphology and biochemistry, so CCl_4 is widely used to induce liver fibrosis or liver injury models, which are often used to explore the anti-fibrotic mechanisms and anti-hepatotoxic (hepatoprotective) activity of synthetic substances or natural products [41]. Therefore, our choice of TGF-β1-stimulated HSCs and CCl_4-induced hepatic fibrosis rat model may have important clinical significance for the elucidation of the mechanisms of PA-B intervention for the treatment of hepatic fibrosis.

Serum activities of AST and ALT are the most basic indices reflecting liver function [42]. HA, LN, PC-III, and Col-IV are the main components of the ECM, which act as important markers for the formation and degree of liver fibrosis in clinical diagnosis. The activity of AST and ALT, together with the serum levels of HA, LN, PC-III, and Col-IV in CCl_4 rats were considerably greater than that of the control group. Colchicine and PA-B reduced the activities of AST and ALT in serum of CCl_4-induced rats, and also decreased the contents of HA, LN, PC-III, and Col-IV. PA-B treatment induced a dose-dependent decrease of liver enzymes serum activities in the hepatic fibrosis rat model. However, only the 120 mg/kg dose of PA-B maintained the levels of AST, ALT, HA, LN, PC-III, and Col-IV to a similar level as that of the control group. These findings implied that PA-B alleviates liver function injury and fibrosis progression in rats with experimental hepatic fibrosis.

Liver damage induced by CCl_4 mainly manifests as hepatic cell necrosis, inflammatory cell infiltration, steatosis, and fibrous hypertrophy. The morphological analysis of liver sections in our experimental model clearly demonstrated these changes. The liver fibrosis in PA-B and colchicine treatment groups was improved to varying degrees; the PA-B (120 mg/kg) group showed the greatest improvement. This suggests that PA-B exhibits a therapeutic effect on CCl_4-induced liver fibrosis in rats.

Col-I and Col-III are the most common collagen types in the ECM of the fibrotic liver. The collagen content can indicate the severity of liver fibrosis, and α-SMA is a key sign of HSCs' activation [43, 44]. HSCs are the main source of ECM in the liver parenchyma, and they are also regulated by the ECM components. Thus, HSCs and ECM appear to be inextricably linked and reciprocally regulate each other [45, 46]. Our study of the cultured HSC-T6 cells incubated with TGF-β1 showed that Col-I and Col-III proteins are mainly uniformly in their cytoplasm or around the cells. At the same time, the expression of α-SMA, Col-I, and Col-III protein decreased in each

drug treatment group *in vitro* and *in vivo*. This indicated that PA-B suppressed α-SMA, Col-I and Col-III production and secretion, inhibited activation of HSCs, and reduced ECM deposition. The mRNA expression levels of α-SMA and Col-I were drastically reduced in the liver of CCl_4-induced rats treated with colchicine and PA-B. These findings further confirmed that PA-B reduces the degree of liver fibrosis.

The TGF-β1/Smad pathway was identified as a vital process of liver fibrosis [47–49]. TGF-β1 initiates cell membrane signaling by binding and activating TβR I on the cell surface. Activated TβR I binds to TβR II to form complex receptors, and amplifies and transmits signals to intracellular Smad proteins [50, 51]. Phosphorylated TβR I activates downstream signaling factors Smad2 and Smad3 to form complexes that aggregate as transcription factors in the nucleus and control the transcription of target genes. Simultaneously, Smad7 acts as a negative feedback regulator by preventing the phosphorylation of Smad2 and Smad3 though competitive binding to phosphorylated TβR I and other pathways; this inhibits transmission of the TGF-β1/Smad signaling pathway [52].

TβR I and TβR II, as cell surface receptors, exhibit specific- and non-specific binding, so they have a relatively high expression. Immunohistochemical results showed that TβR I and TβR II proteins were highly expressed on the surface of HSC-T6 cells, especially in the TGF-β1 stimulated group. Smad2 and Smad3 intracellular signaling proteins were mainly expressed in the nucleus, and their expression levels were lower than that of receptor proteins. LY-364947 was selected as a selective ATP-competitive TGF-β receptor kinase I inhibitor [53]. The LY-364947 and PA-B drug groups downregulated the mRNA and protein expressions of TβR I, TβR II, Smad2, and Smad3. Meanwhile, the mRNA and protein levels of antagonistic factor Smad7 decreased. This suggests that PA-B inhibits the TGF-β1/Smad signaling pathway by interfering with the expression of TβR I, TβR II, Smad2, Smad3, and Smad7 in HSC-T6 cells. *In vivo* experiments confirmed that PA-B and colchicine decrease the expression of TβR I, TβR II, Smad2, Smad3, and TGF-β1 in rat liver tissue, and increase Smad7 expression to inhibit the TGF-β1/Smad signaling pathway. The result showed that PA-B plays an anti-fibrosis role by inhibiting the TGF-β1/Smad signaling pathway in a dose-dependent manner, and inhibiting the synthesis and secretion of α-SMA, Col-I, and Col-III in HSC-T6 cells.

In conclusion, this study demonstrated the anti-fibrotic effects of PA-B in *in vitro* and *in vivo* liver fibrosis models by interfering with TGF-β1secretion, reducing collagen synthesis, and regulating the TGF-β1/Smad signaling pathway. Overall, these results suggest that the TGF-β1/Smad signaling pathway is a possible molecular mechanism of the PA-B antifibrotic effect in rat liver. However, PA-B is an active extract of *P. americana* containing multiple components, so its mechanism of action may involve multiple targets and the joint action of multiple signaling

pathways.

Article information

Ethics statement

This study protocol was reviewed and approved by the ethics committee of Dali University (28 June 2021, 2021-PZ-019) and the project is considered to be in line with medical ethics.

Author contributions

Yi Chen: Methodology, writing original draft preparation, investigation, formal analysis, data curation. **Yanwen Zhao**: Methodology software. **Ying He**; **Liping Yuan**: Supervision, conceptualization, funding acquisition. **Yongshou Yang**: writing review and editing. **Peiyun Xiao**: Validation, formal analysis, writing review and editing. All authors have read and agree to the published version of the manuscript.

Funding

This research was supported by the National Natural Science Foundation of China [81560634, 82060747] and Basic Research Projects of Local Undergraduate Universities in Yunnan Province [2019FH001-034].

Conflict of interest

The authors declare that they have no conflict of interest.

References

1. Shan L, Wang F, Zhai D, et al. New Drugs for Hepatic Fibrosis. Front Pharmacol. 2022; 13: 874408, doi: 10.3389/fphar.2022.874408, indexed in Pubmed: 35770089.

2. Roehlen N, Crouchet E, Baumert TF. Liver fibrosis: mechanistic concepts and therapeutic perspectives. Cells. 2020; 9(4), doi: 10.3390/cells9040875, indexed in Pubmed: 32260126.

3. Wang YH, Twu YC, Wang CK, et al. Niemann-Pick type C2 protein regulates free cholesterol accumulation and influences hepatic stellate cell proliferation and mitochondrial respiration function. Int J Mol Sci. 2018; 19(6), doi: 10.3390/ijms19061678, indexed in Pubmed: 29874879.

4. Lu P, Yan M, He Li, et al. Crosstalk between epigenetic modulations in valproic acid deactivated hepatic stellate cells: an integrated protein and miRNA profiling study. Int J Biol Sci. 2019; 15(1): 93–104, doi: 10.7150/ijbs.28642, indexed in Pubmed: 30662350.

5. Lo RC, Kim H. Histopathological evaluation of liver fibrosis and cirrhosis regression. Clin Mol Hepatol. 2017; 23(4): 302–307, doi: 10.3350/cmh.2017.0078, indexed in Pubmed: 29281870.
6. Tsuchida T, Friedman SL. Mechanisms of hepatic stellate cell activation. Nat Rev Gastroenterol Hepatol. 2017; 14(7): 397–411, doi: 10.1038/nrgastro.2017.38, indexed in Pubmed: 28487545.
7. Zhangdi HJ, Su SB, Wang F, et al. Crosstalk network among multiple inflammatory mediators in liver fibrosis. World J Gastroenterol. 2019; 25(33): 4835–4849, doi: 10.3748/wjg.v25.i33.4835, indexed in Pubmed: 31543677.
8. Li D, Ma D, Liu Ye, et al. Extracts of Periplaneta americana alleviate hepatic fibrosis by affecting hepatic TGF-β and NF-κB expression in rats with pig serum-induced liver fibrosis. Folia Histochem Cytobiol. 2022; 60(2): 125–135, doi: 10.5603/FHC.a2022.0011, indexed in Pubmed: 35575220.
9. Inagaki Y, Okazaki I. Emerging insights into Transforming growth factor beta Smad signal in hepatic fibrogenesis. Gut. 2007; 56(2): 284–292, doi: 10.1136/gut.2005.088690, indexed in Pubmed: 17303605.
10. Sun WY, Gu YJ, Li XR, et al. β-arrestin2 deficiency protects against hepatic fibrosis in mice and prevents synthesis of extracellular matrix. Cell Death Dis. 2020; 11(5): 389, doi: 10.1038/s41419-020-2596-8, indexed in Pubmed: 32439968.
11. Loboda A, Sobczak M, Jozkowicz A, et al. TGF-β1/Smads and miR-21 in renal fibrosis and inflammation. Mediators Inflamm. 2016; 2016: 8319283, doi: 10.1155/2016/8319283, indexed in Pubmed: 27610006.
12. Chen L, Yang T, Lu DW, et al. Central role of dysregulation of TGF-β/Smad in CKD progression and potential targets of its treatment. Biomed Pharmacother. 2018; 101: 670–681, doi: 10.1016/j.biopha.2018.02.090, indexed in Pubmed: 29518614.
13. Jiang Y, Xiang C, Zhong F, et al. Histone H3K27 methyltransferase EZH2 and demethylase JMJD3 regulate hepatic stellate cells activation and liver fibrosis. Theranostics. 2021; 11(1): 361–378, doi: 10.7150/thno.46360, indexed in Pubmed: 33391480.
14. Saito A, Horie M, Nagase T. TGF-β signaling in lung health and disease. Int J Mol Sci. 2018; 19(8), doi: 10.3390/ijms19082460, indexed in Pubmed: 30127261.

15. Hahn O, Ingwersen LC, Soliman A, et al. TGF-ß1 induces changes in the energy metabolism of white adipose tissue-derived human adult mesenchymal stem/stromal cells . Metabolites. 2020; 10(2), doi: 10.3390/metabo10020059, indexed in Pubmed: 32046088.
16. He X, Cheng R, Huang C, et al. A novel role of LRP5 in tubulointerstitial fibrosis through activating TGF-β/Smad signaling. Signal Transduct Target Ther. 2020; 5(1): 45, doi: 10.1038/s41392-020-0142-x, indexed in Pubmed: 32345960.
17. Yoshida K, Murata M, Yamaguchi T, et al. TGF-β/Smad signaling during hepatic fibro-carcinogenesis (review). Int J Oncol. 2014; 45(4): 1363–1371, doi: 10.3892/ijo.2014.2552, indexed in Pubmed: 25050845.
18. Cheng Qi, Li C, Yang CF, et al. Methyl ferulic acid attenuates liver fibrosis and hepatic stellate cell activation through the TGF-β1/Smad and NOX4/ROS pathways. Chem Biol Interact. 2019; 299: 131–139, doi: 10.1016/j.cbi.2018.12.006, indexed in Pubmed: 30543783.
19. Yang YX, Luo Qi, Hou Bo, et al. Periplanosides A-C: new insect-derived dihydroisocoumarin glucosides from Periplaneta americana stimulating collagen production in human dermal fibroblasts. J Asian Nat Prod Res. 2015; 17(10): 988–995, doi: 10.1080/10286020.2015.1047771, indexed in Pubmed: 26499169.
20. Yun J, Hwang JS, Lee DG. The antifungal activity of the peptide, periplanetasin-2, derived from American cockroach . Biochem J. 2017; 474(17): 3027–3043, doi: 10.1042/BCJ20170461, indexed in Pubmed: 28733329.
21. Gao Y, Liang LC, Wang R, et al. Chemical constituents from Periplaneta americana. Chin Tradit Patent Med. 2018; 40: 375–378.
22. Si JG, Zhang T, Li LY, et al. Chemical constituents from Periplaneta Americana. Chin Pharm J. 2018; 53(3): 178–181.
23. Wang Q, Liu K, Kong C, et al. Current situation on antioxidant stress and active compounds of Periplaneta americana extracts. Chin Arch Tradi Chin Med. 2021; 39: 124–127, doi: 10.13193/j.issn.1673-7717.2021.07.032.
24. Gao YY, Geng FN, Chen SM, et al. Advances in research on active ingredients and related pharmacology of Periplaneta americana. Chin J Exp Tradit Med Form. 2021; 24: 240–250, doi: 10.13422/j.cnki.syfjx.20210245.

25. Gu T, Yang YS, Xie JJ, et al. Effects of active extracts from Periplaneta Americana on treating hepatic fibrosis in rats by gastric and intestinal administration. J Dali Univ. 2021; 6: 18–22.
26. Fu W, Zhao Y, Xie J, et al. Identification of anti-hepatic fibrosis components in Periplaneta americana based on spectrum-effect relationship and chemical component separation. Biomed Chromatogr. 2022; 36(3): e5286, doi: 10.1002/bmc.5286, indexed in Pubmed: 34837247.
27. Naik N, Madani A, Esteva A, et al. Deep learning-enabled breast cancer hormonal receptor status determination from base-level H&E stains. Nat Commun. 2020; 11(1): 5727, doi: 10.1038/s41467-020-19334-3, indexed in Pubmed: 33199723.
28. Iezzoni JC. Diagnostic histochemistry in hepatic pathology. Semin Diagn Pathol. 2018; 35(6): 381–389, doi: 10.1053/j.semdp.2018.10.003, indexed in Pubmed: 30409459.
29. Ghasemzadeh N, Pourrajab F, Dehghani Firoozabadi A, et al. Ectopic microRNAs used to preserve human mesenchymal stem cell potency and epigenetics. EXCLI J. 2018; 17: 576–589, doi: 10.17179/excli2018-1274, indexed in Pubmed: 30108462.
30. Shi WP, Ju Di, Li H, et al. CD147 promotes CXCL1 expression and modulates liver fibrogenesis. Int J Mol Sci. 2018; 19(4), doi: 10.3390/ijms19041145, indexed in Pubmed: 29642635.
31. Seki E, Schwabe RF. Hepatic inflammation and fibrosis: functional links and key pathways. Hepatology. 2015; 61(3): 1066–1079, doi: 10.1002/hep.27332, indexed in Pubmed: 25066777.
32. Ezhilarasan D, Sokal E, Najimi M. Hepatic fibrosis: It is time to go with hepatic stellate cell-specific therapeutic targets. Hepatobiliary Pancreat Dis Int. 2018; 17(3): 192–197, doi: 10.1016/j.hbpd.2018.04.003, indexed in Pubmed: 29709350.
33. Shi W, An Li, Zhang J, et al. extract ameliorates lipopolysaccharide-induced liver injury by improving mitochondrial dysfunction via the AMPK/PGC-1α signaling pathway. Exp Ther Med. 2021; 22(4): 1138, doi: 10.3892/etm.2021.10572, indexed in Pubmed: 34504584.
34. Yuan L, Yang X, He Y, et al. Mechanism of the anti-liver fibrosis effect of Periplaneta americana extracts that promote apoptosis of HSC-T6 cells through the Bcl-2/Bax signaling pathway. J Asia-Pac Entomol. 2023; 26(2): 102094, doi: 10.1016/j.aspen.2023.102094.
35. Gasparyan AY, Ayvazyan L, Yessirkepov M, et al. Colchicine as an anti-inflammatory and cardioprotective agent. Expert Opin Drug Metab Toxicol. 2015; 11(11): 1781–1794, doi: 10.1517/17425255.2015.1076391, indexed in Pubmed: 26239119.

36. Liu H, Zhang Z, Hu H, et al. Protective effects of Liuweiwuling tablets on carbon tetrachloride-induced hepatic fibrosis in rats. BMC Complement Altern Med. 2018; 18(1): 212, doi: 10.1186/s12906-018-2276-8, indexed in Pubmed: 29986685.
37. López-Hernández FJ, López-Novoa JM. Role of TGF-β in chronic kidney disease: an integration of tubular, glomerular and vascular effects. Cell Tissue Res. 2012; 347(1): 141–154, doi: 10.1007/s00441-011-1275-6, indexed in Pubmed: 22105921.
38. Song L, Qu D, Zhang Q, et al. Phytosterol esters attenuate hepatic steatosis in rats with non-alcoholic fatty liver disease rats fed a high-fat diet. Sci Rep. 2017; 7: 41604, doi: 10.1038/srep41604, indexed in Pubmed: 28169366.
39. Yanguas SC, Cogliati B, Willebrords J, et al. Experimental models of liver fibrosis. Arch Toxicol. 2016; 90(5): 1025–1048, doi: 10.1007/s00204-015-1543-4, indexed in Pubmed: 26047667.
40. Tang G, Seume N, Häger C, et al. Comparing distress of mouse models for liver damage. Sci Rep. 2020; 10(1): 19814, doi: 10.1038/s41598-020-76391-w, indexed in Pubmed: 33188220.
41. Manibusan MK, Odin M, Eastmond DA. Postulated carbon tetrachloride mode of action: a review. J Environ Sci Health C Environ Carcinog Ecotoxicol Rev. 2007; 25(3): 185–209, doi: 10.1080/10590500701569398, indexed in Pubmed: 17763046.
42. Tabrez S, Ahmad M. Effect of wastewater intake on antioxidant and marker enzymes of tissue damage in rat tissues: implications for the use of biochemical markers. Food Chem Toxicol. 2009; 47(10): 2465–2478, doi: 10.1016/j.fct.2009.07.004, indexed in Pubmed: 19596398.
43. Liang L, Yang X, Yu Y, et al. Babao Dan attenuates hepatic fibrosis by inhibiting hepatic stellate cells activation and proliferation via TLR4 signaling pathway. Oncotarget. 2016; 7(50): 82554–82566, doi: 10.18632/oncotarget.12783, indexed in Pubmed: 27776340.
44. Stanko P, Baka T, Repova K, et al. Ivabradine Ameliorates Kidney Fibrosis in L-NAME-Induced Hypertension. Front Med (Lausanne). 2020; 7: 325, doi: 10.3389/fmed.2020.00325, indexed in Pubmed: 32754607.
45. Chen X, Li HD, Bu FT, et al. Circular RNA circFBXW4 suppresses hepatic fibrosis via targeting the miR-18b-3p/FBXW7 axis. Theranostics. 2020; 10(11): 4851–4870, doi: 10.7150/thno.42423, indexed in Pubmed: 32308754.

46. Dawood RM, El-Meguid MA, Salum GM, et al. Key players of hepatic fibrosis. J Interferon Cytokine Res. 2020; 40(10): 472–489, doi: 10.1089/jir.2020.0059, indexed in Pubmed: 32845785.
47. Yang HY, Kim KS, Lee YH, et al. Ameliorates Thioacetamide-Induced Hepatic Fibrosis via TGF-β1/Smads Pathways. Int J Biol Sci. 2019; 15(4): 800–811, doi: 10.7150/ijbs.30356, indexed in Pubmed: 30906211.
48. Zhang L, Liu C, Meng XM, et al. Smad2 protects against TGF-β1/Smad3-mediated collagen synthesis in human hepatic stellate cells during hepatic fibrosis. Mol Cell Biochem. 2015; 400(1-2): 17–28, doi: 10.1007/s11010-014-2258-1, indexed in Pubmed: 25351340.
49. Xu F, Liu C, Zhou D, et al. TGF-β/SMAD pathway and its regulation in hepatic fibrosis. J Histochem Cytochem. 2016; 64(3): 157–167, doi: 10.1369/0022155415627681, indexed in Pubmed: 26747705.
50. Sferra R, Vetuschi A, Pompili S, et al. Expression of pro-fibrotic and anti-fibrotic molecules in dimethylnitrosamine-induced hepatic fibrosis. Pathol Res Pract. 2017; 213(1): 58–65, doi: 10.1016/j.prp.2016.11.004, indexed in Pubmed: 27894619.
51. Yang N, Dang S, Shi J, et al. Caffeic acid phenethyl ester attenuates liver fibrosis via inhibition of TGF-β1/Smad3 pathway and induction of autophagy pathway. Biochem Biophys Res Commun. 2017; 486(1): 22–28, doi: 10.1016/j.bbrc.2017.02.057, indexed in Pubmed: 28193525.
52. Hu HH, Chen DQ, Wang YN, et al. New insights into TGF-β/Smad signaling in tissue fibrosis. Chem Biol Interact. 2018; 292: 76–83, doi: 10.1016/j.cbi.2018.07.008, indexed in Pubmed: 30017632.
53. Ebeid DE, Khalafalla FG, Broughton KM, et al. Pim1 maintains telomere length in mouse cardiomyocytes by inhibiting TGFβ signalling. Cardiovasc Res. 2021; 117(1): 201–211, doi: 10.1093/cvr/cvaa066, indexed in Pubmed: 32176281.

Table 1. PCR primer sequences

Gene	Forward	Reverse
GAPDH	5'-GGGGCTCTCTGCTCCTCCCTG-3'	5'-CGGCCAAATCCGTTCACACCG-3'
α-SMA	5'-CAGCCAGTCGCCATCAGGAAC-3'	5'-CCAGCAAAGCCCGCCTTACAG-3'
Col-I	5'-TGTTGGTCCTGCTGGCAAGAATG-3'	5'-GTCACCTTGTTCGCCTGTCTCAC-3'
TβR I	5'-GCTCTGGGCAAAGATTAGGGTGAC-3'	5'-GCAGGATTACAGGCTCAGCTCATC-3'
TβR II	5'-AATGAAGAATACACCACCAGCAGTCC-3'	5'-ACGGTAACAGTAGAAGATGGCAATGAC-3'
Smad2	5'-ATGTCGTCCATCTTGCCATTCACTC-3'	5'-CATTCTGTTCTCCACCACCTGCTC-3'
Smad3	5'-AACCACAGAAGATGCCAGCGATG-3'	5'-GCCACCAGATCAGAAGCCATCAC-3'
Smad7	5'-CAGCCGCCCTCGTCCTACTC-3'	5'-ACAGCAACACAGCCTCTTGACTTC-3'
TGF-β1	5'-GCAACAATTCCTGGCGTTACCTTG-3'	5'-GTATTCCGTCTCCTTGGTTCAGC-3'

Table 2. Identification of nine compounds purified from *Periplaneta americana* extract (PA-B) by semi-preparative high performance liquid chromatography

No.	t_R (min)	Formula	Identification
S1	18.440	$C_{20}H_{36}O_4$	9,12-heptadecanedenoic acid glyceride
S2	21.198	$C_{20}H_{40}O_2$	Nonadecanoic acid methyl ester
S3	22.864	$C_{21}H_{40}O_4$	Glyceryl oleate
S4	24.295	$C_{25}H_{44}O_2$	13,16,19-eicosatrienoic acid

S5	28.670	$C_{21}H_{36}O_4$	9,12,15-octadecatrienoic acid glyceride
S6	31.922	$C_{18}H_{32}O_2$	Linoleic acid
S7	38.528	$C_{16}H_{32}O_2$	Hexadecanoic acid
S8	43.384	$C_{18}H_{34}O_2$	Oleic acid
S9	61.260	$C_{18}H_{36}O_2$	Octadecanoic acid

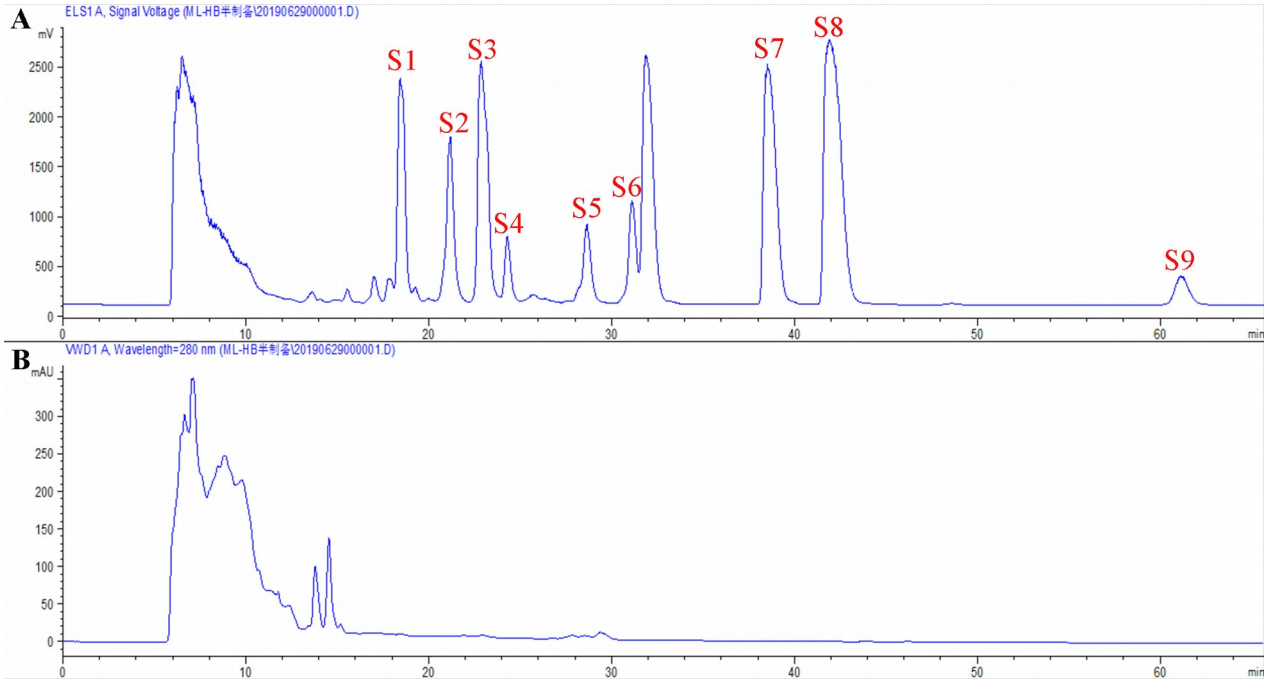

Figure 1. Chromatogram of *Periplaneta americana* extract (PA-B) semi-preparation by HPLC-VWD (280 nm)-ELSD. **A.** Evaporative light signal. **B.** Ultraviolet light signal.

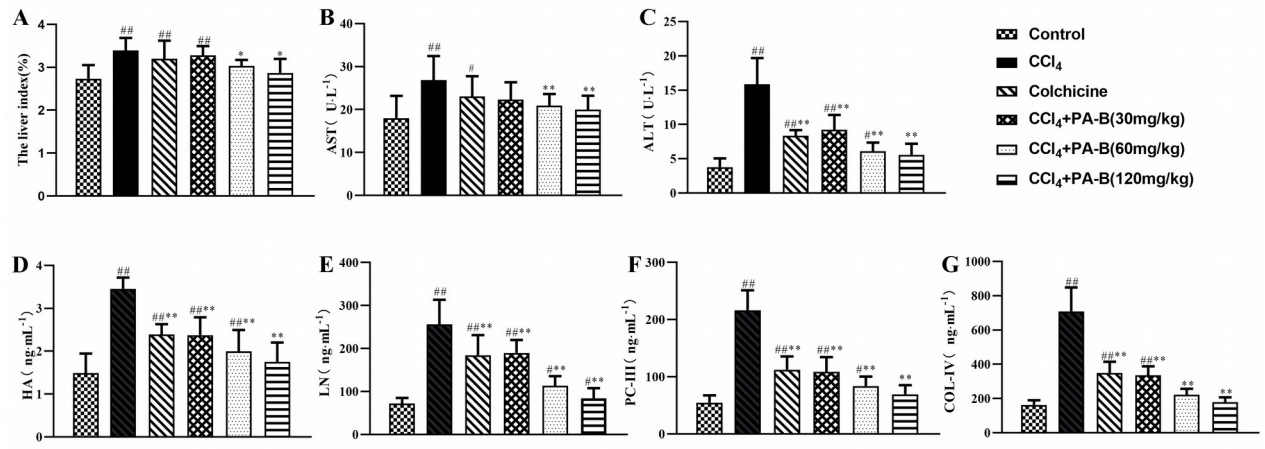

Figure 2. Effects of CCl_4, colchicine and *Periplaneta americana* extract (PA-B) on the liver organ index, serum liver function index and liver fibrosis index. Male rats received CCl_4 in a total dose of 15 mL/kg over six weeks, and then they received indicated doses of PA-B for four weeks. Additional group of animals received CCl_4 for six weeks and then they received colchicine (0.2 mg/kg) for four weeks. **A.** Liver weight index. **B.** Serum AST activity. **C.** Serum ALT activity. **D–G.** Serum concentrations of hyaluronic acid (HA), laminin (LN), procollagen III (PC-III) and collagen type IV (Col-IV), respectively. Data are expressed as the mean ± standard deviation (SD) (n = 8). $^{\#}P < 0.05$ and $^{\#\#}P < 0.01$, *vs.* control; $^{*}P < 0.05$ and $^{**}P < 0.01$, *vs.* CCl_4.

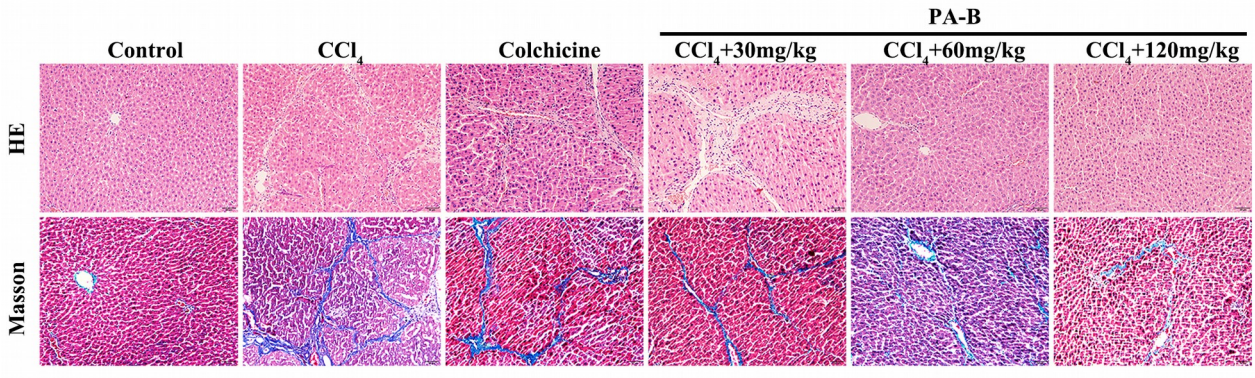

Figure 3. Representative microphotographs of hematoxylin and eosin- and Masson-stained liver sections of rats treated with CCl_4 for six weeks, and then with colchicine or PA-B for four weeks at the doses provided in the legend to Fig. 2. Magnification: 200×.

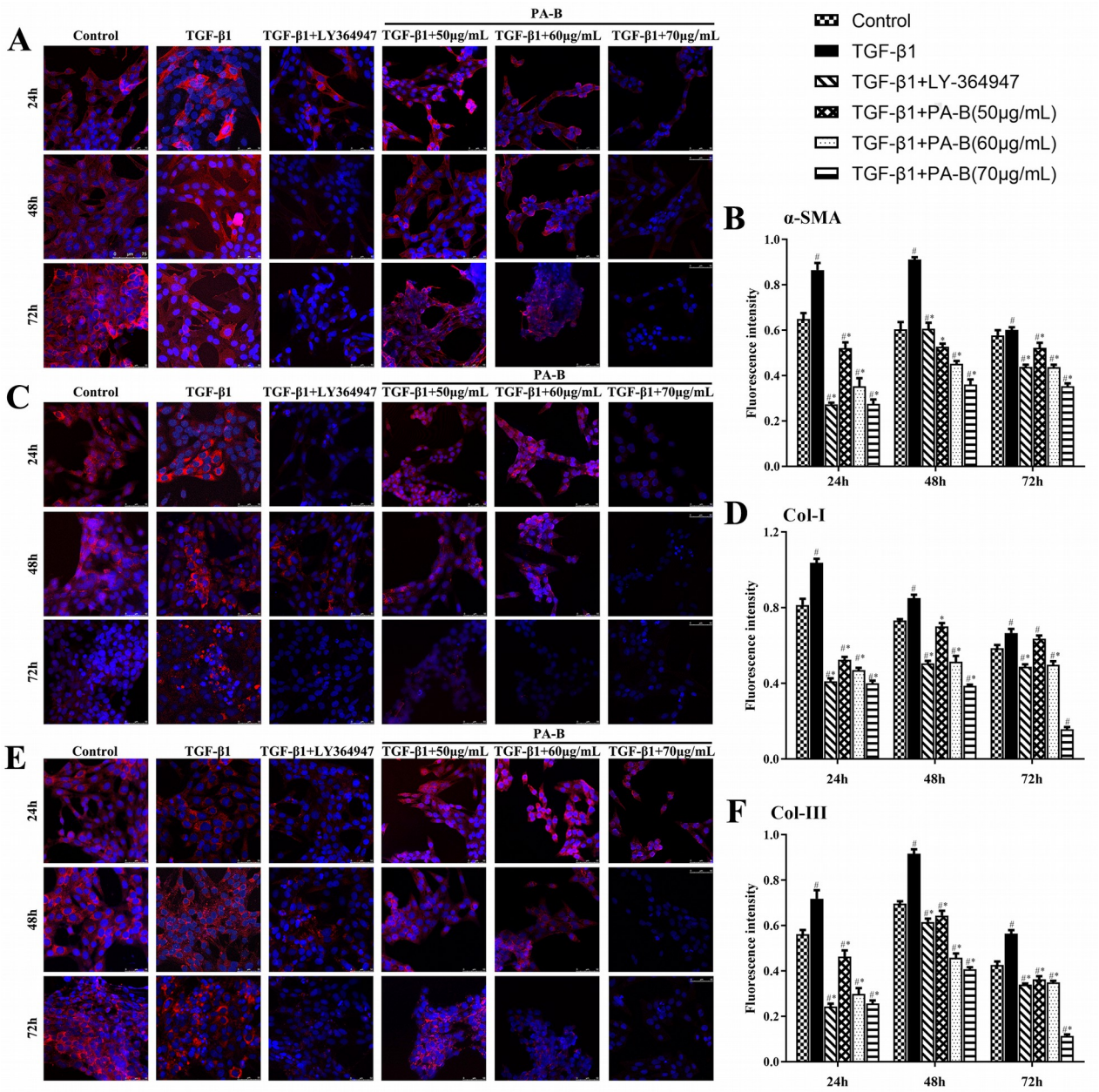

Figure 4. Effects of TGF-β1, PA-B and LY-364947 on α-smooth-muscle actin (α-SMA), collagen type I (COL-I), and collagen type III (COL-III) expression in cultures of hepatic stellate HSC-T6 cells. **A.** Immunofluorescence of α-SMA at 24, 48, and 72 h. **B.** Protein expression of α-SMA at 24, 48, and 72 h. **C.** Immunofluorescence of Col-I at 24, 48 and 72 h. **D.** Protein expression of Col-I at 24, 48 and 72 h. **E.** Immunofluorescence of Col-III at 24, 48, and 72 h. **F.** Protein expression of Col-III at 24, 48, and 72 h. Cell nuclei were stained blue with DAPI. Scale bar: 50 μm. Data are expressed as the mean ± standard deviation (n = 5). $^{\#}P < 0.05$ and $^{\#\#}P < 0.01$, *vs.* the Control; $^{*}P < 0.05$ and $^{**}P < 0.01$, *vs.* LY-364947.

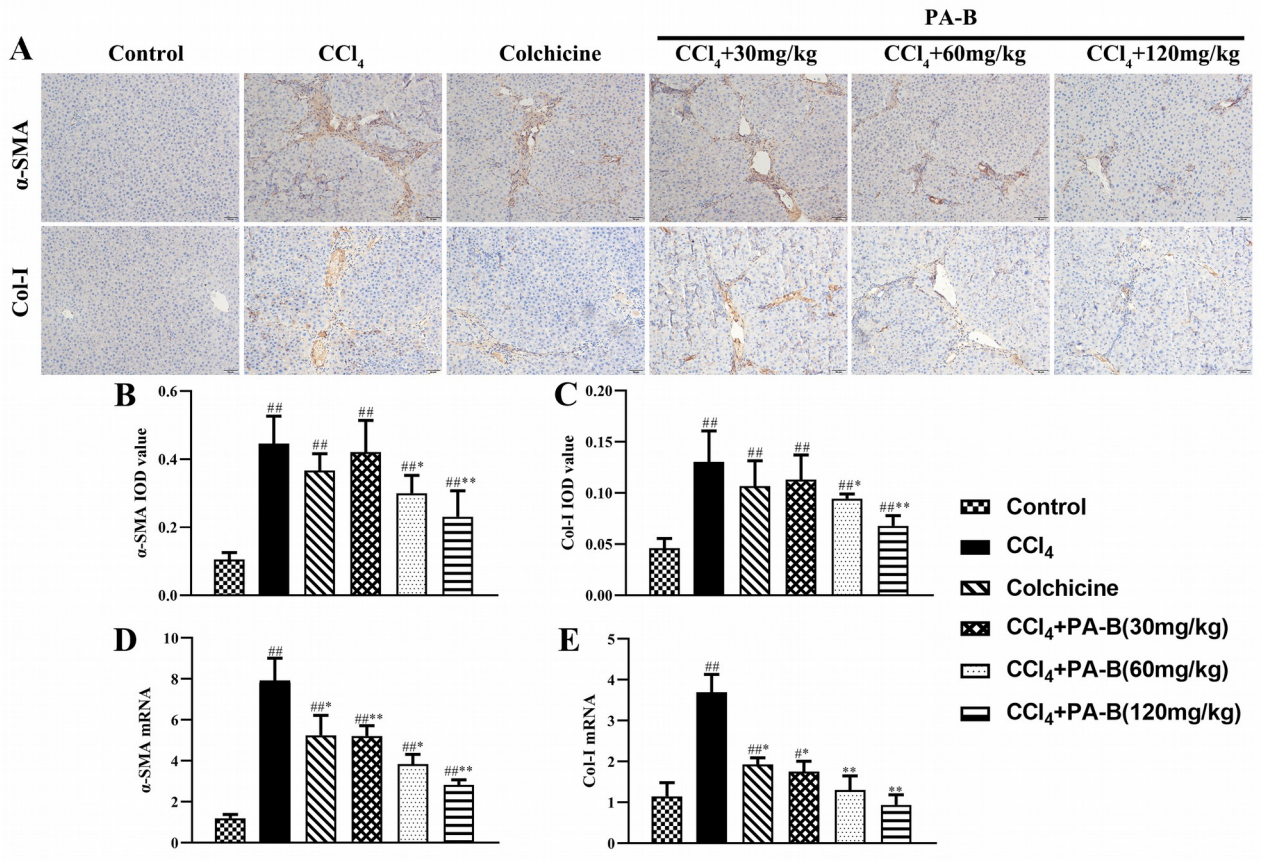

Figure 5. PA-B inhibits α-smooth-muscle actin (α-SMA) and collagen expression in CCl_4-induced liver fibrosis in rats. **A.** Immunohistochemical images. **B.** Integrated optical density (IOD) of α-SMA in liver tissue. C. IOD of Col-I in liver tissue. **D.** Expression of α-SMA mRNA in liver tissue. **E.** Expression of Col-I mRNA in liver tissue. Magnification: 200×. Data are expressed as the mean ± standard deviation (n = 5). $^{\#}P < 0.05$ and $^{\#\#}P < 0.01$ *vs.* the Control; $^{*}P < 0.05$ and $^{**}P < 0.01$, *vs.* CCl_4 group.

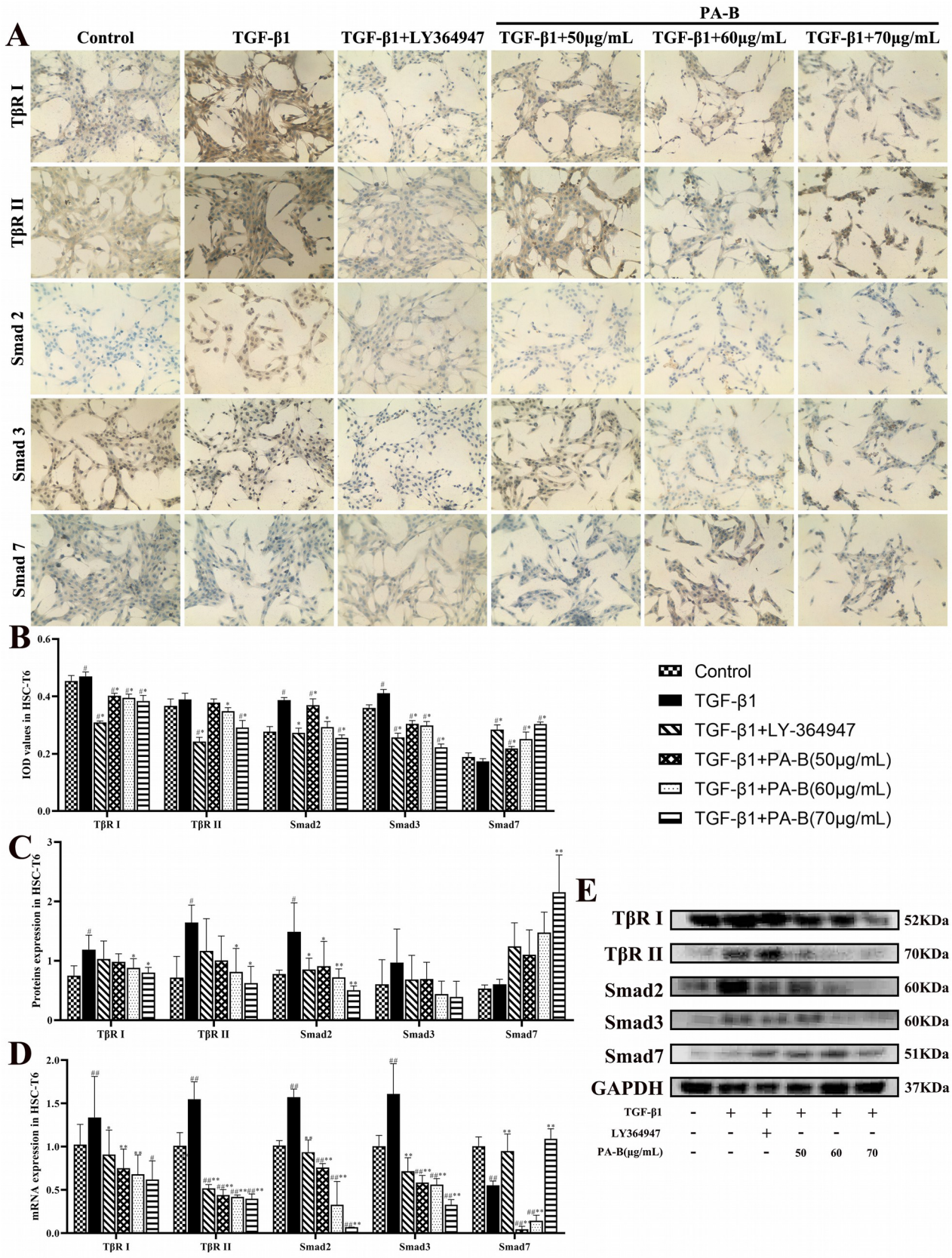

Figure 6. Effects of PA-B on the expression of TGF-β/Smad signaling pathway in TGF-β1-treated HSC-T6 cells. **A.** Immunohistochemical demonstration of TβR I, TβR II, Smad2, Smad3, and Smad7. Scale bar: 50 μm. **B.** IOD value of TβR I, TβR II, Smad2, Smad3, and Smad7 in HSC-T6

cells (n = 5). **C.** Protein expression of TβR I, TβR II, Smad2, Smad3, and Smad7 (n = 3). **D.** mRNA expression of TβR I, TβR II, Smad2, Smad3, and Smad7 (n = 5). **E.** Western blots of TβR I, TβR II, Smad2, Smad3, and Smad7. Data are expressed as the mean ± standard deviation. $^{\#}P < 0.05$ and $^{\#\#}P < 0.01$, *vs.* the Control; $^{*}P < 0.05$ and $^{**}P < 0.01$, *vs.* LY-364947. Abbreviation: IOD — integrated optical density.

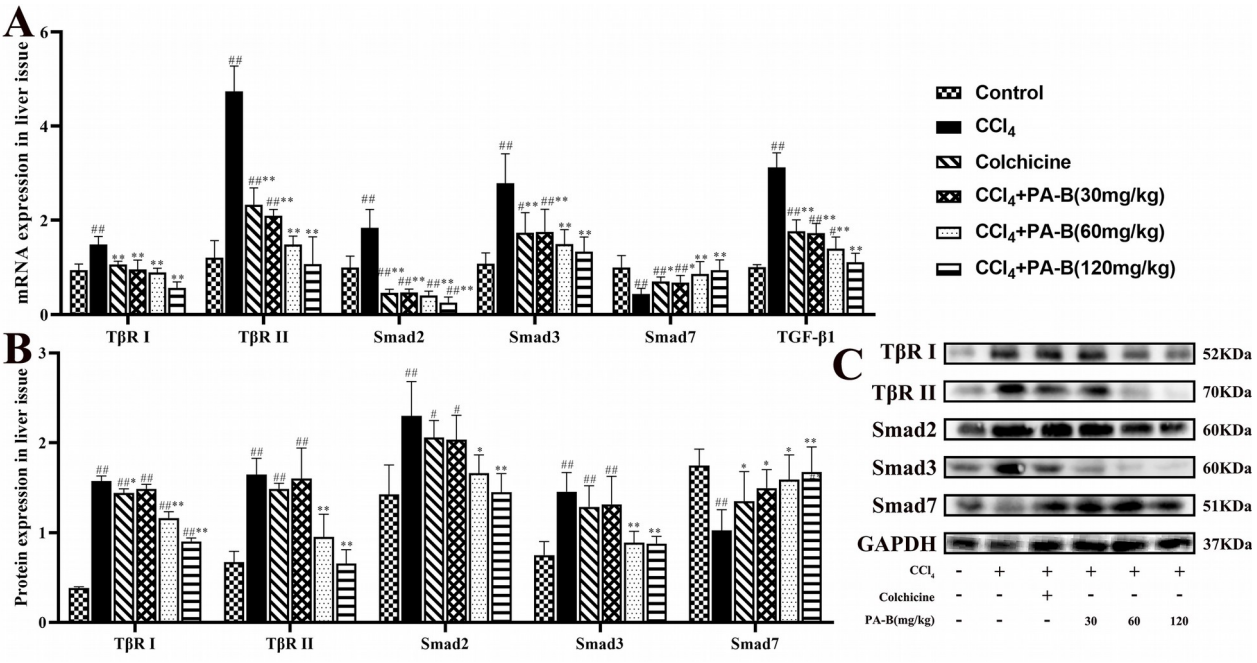

Figure 7. Effects of PA-B on the expression of the TGF-β/Smad signaling pathway in CCl_4-induced rat liver fibrosis. **A.** Relative mRNA expression of TβR I, TβR II, Smad2, Smad3, Smad7, and TGF-β1 in CCl_4 (n = 5). **B.** Protein expression of TβR I, TβR II, Smad2, Smad3, and Smad7 (n = 3). **C.** Western blot of TβR I, TβR II, Smad2, Smad3, and Smad7. Data are expressed as the mean ± standard deviation. $^{\#}P < 0.05$ and $^{\#\#}P < 0.01$, *vs.* the Control; $^{*}P < 0.05$ and $^{**}P < 0.01$, *vs.* CCl_4.